nature communications

Article

https://doi.org/10.1038/s41467-024-54949-w

Time-resolved X-ray solution scattering unveils the events leading to hemoglobin heme capture by staphylococcal IsdB

Received: 29 August 2023

Accepted: 25 November 2024

Published online: 17 February 2025

Check for updates

Omar De Bei[1], Marialaura Marchetti[1], Stefano Guglielmo[2], Eleonora Gianquinto[2], Francesca Spyrakis[2], Barbara Campanini[3], Stefano Bettati[1,4], Matteo Levantino[5] ✉ & Luca Ronda[1,4] ✉

Infections caused by *Staphylococcus aureus* depend on its ability to acquire nutrients. One essential nutrient is iron, which is obtained from the heme of the human host hemoglobin (Hb) through a protein machinery called Iron-regulated surface determinant (Isd) system. IsdB is the protein in charge of heme extraction from Hb, which is the first step of the chain of events leading to iron transfer to the bacterium cell interior. In order to elucidate the molecular events leading from the formation of the initial IsdB:Hb complex to heme extraction, we use time-resolved X-ray solution scattering (TR-XSS) in combination with rapid mixing triggering. We succeed in defining the stoichiometry of IsdB:Hb binding and in describing the kinetics of the subsequent structural changes. The presented approach is potentially applicable to unveil the complex kinetic pathways generated by protein-protein interaction in different biological systems.

The interaction between macromolecules guides and regulates all fundamental processes in living organisms. Identifying and characterizing these interactions in detail is a major challenge in life sciences, continuously calling for alternative approaches. A particularly important role is played by protein-protein interactions (PPIs) in cellular processes within a given organism, or when different organisms get in contact, as in the attack of a pathogen to a host organism, where bacterial invasion and proliferation often relies on specific PPIs. A relevant example of the latter is present in *Staphylococcus aureus* infections in human host[1]. One of the bacterial first needs for a successful infection is the access to iron, whose primary supply is represented by the hemic cofactor of hemoglobin (Hb). To fulfill its nutritional requirements, *S. aureus* has evolved an arsenal of hemolysins to disrupt erythrocyte membrane and an Iron-regulated surface determinant (Isd) system, composed of nine proteins (IsdA-I) to bind Hb, scavenge heme and acquire iron (Fig. 1)[2]. Several Isd proteins are cell-wall exposed and, in particular, IsdB and IsdH are in charge of extracellular Hb interception; apparently, the two receptors play a superimposable function, but only IsdB is classified as a virulence factor[3], eliciting a primary interest in the detailed comprehension of its mechanism of interaction with Hb. IsdB is a flexible, modular protein composed of two immunoglobulin-like domains called NEAr iron Transporter (NEAT), separated by a linker conferring mobility to the protein. The heme extraction process proceeds in two phases: the interaction between IsdB and Hb initially occurs through the NEAT1 domain and is followed by the heme transfer from Hb to the bacterial receptor, operated by its NEAT2[4–8]. Interfering with this mechanism is an attractive way to starve the bacterium and impair its proliferation, and represents an alternative novel explorable target for developing antimicrobial agents against *S. aureus* and its multidrug-resistant strains, ranked by the World Health Organization as high-priority in the search of antibiotics[9,10].

The biological relevance of the PPI between IsdB and Hb motivated us in pursuing an in-depth investigation of the dynamics of the

[1]Department of Medicine and Surgery, University of Parma, Via Volturno, 39, Parma, Italy. [2]Department of Drug Science and Technology, University of Turin, Via Giuria, 9, Turin, Italy. [3]Department of Food and Drug, University of Parma, Parco Area delle Scienze, 27/A, Parma, Italy. [4]Institute of Biophysics, CNR, Via G. Moruzzi, 1, Pisa, Italy. [5]ESRF - The European Synchrotron, 71 Avenue des Martyrs, CS40220, 38043, Grenoble, Cedex, France.
✉e-mail: matteo.levantino@esrf.fr; luca.ronda@unipr.it

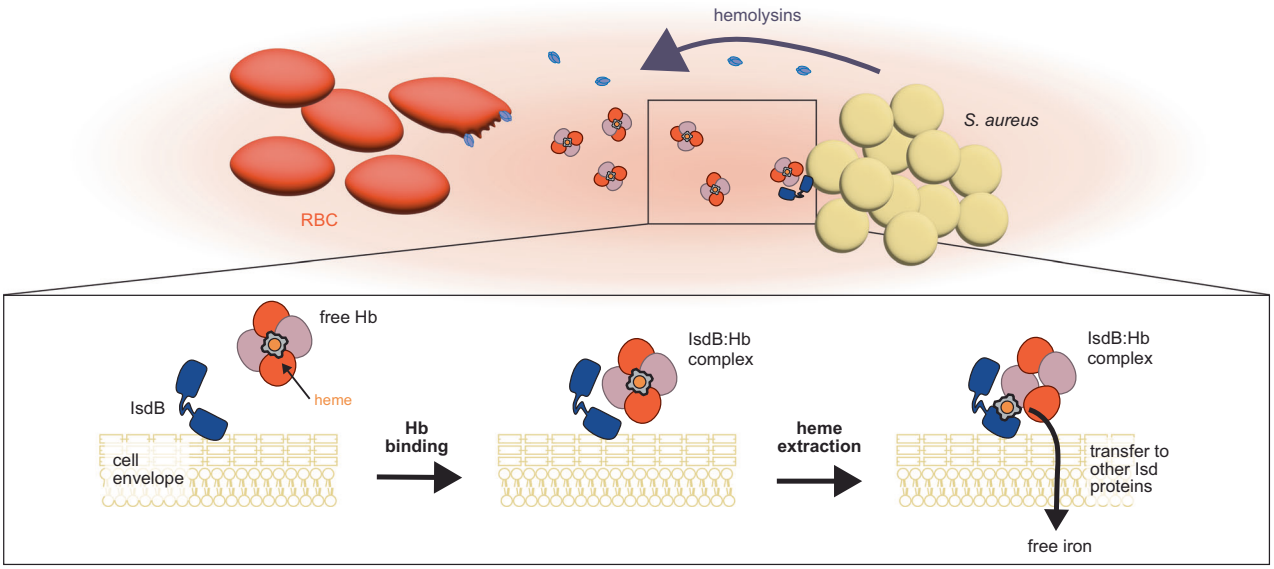

Fig. 1 | Schematic representation of the interaction between *Staphylococcus aureus* and human host for the bacterial acquisition of iron. The bacterium produces hemolysins to lyse red blood cells (RBC) and release Hb. To proceed with the iron acquisition, *S. aureus* exposes the Hb receptor IsdB outside the cell wall. The magnified region shows how IsdB mediates the first step in iron acquisition: IsdB binds free Hb in the bloodstream, extracts heme and then passes it to the following proteins of the Isd system for its degradation and iron release.

whole process leading from the formation of the complex between IsdB and Hb (IsdB:Hb) to heme extraction. Up to now, this process has been extrapolated indirectly from optical spectroscopy data and available structures of IsdB:Hb complexes[6–8]. By performing time-resolved X-ray solution scattering (TR-XSS) measurements after rapid mixing of *S. aureus* IsdB with human Hb we have been able to elucidate important steps in this prototypical PPI with a direct structural sensitive technique. Although XSS yields lower resolution data than X-ray crystallography, it can be applied to track in real time structural changes in solution that cannot take place within a crystal[11]. Being directly sensitive to structural rearrangements of proteins at the tertiary and quaternary level[11,12], TR-XSS has been successfully applied to investigate several biologically relevant structural relaxations including the allosteric transition of human Hb[13–15], the structural dynamics of light-driven proton pumps like bacteriorhodopsin or proteorhodopsin[16,17], the ultrafast "protein quake" of myoglobin[18–20] or the photoactivation processes of phytochromes[21,22] and histidine kinases[23]. More recently, the technique has also been applied to proteins that are not intrinsically photosensitive by employing either photocaged compounds[24–26] or IR laser pulses to induce fast temperature jumps in the solvent[27–31]. All of the above studies have employed a pump-probe approach with a laser pulse trigger followed by an X-ray probe pulse. An alternative possibility that could be applicable to a vastly larger class of biological systems is to follow the X-ray scattering pattern of a sample as a function of time after rapid mixing of two solutions. Although TR-XSS has been already used in combination with a stopped-flow apparatus, all those studies have so far been limited to the small-angle X-ray scattering (SAXS) region[32–36], which mainly yields information on the overall shape of the protein and its radius of gyration.

Here, we show that the structural resolution of this approach can be improved by collecting TR-XSS data in the wide-angle X-ray scattering (WAXS) region after rapidly mixing solutions of IsdB and metHb. Indeed, this approach allows us to follow, in solution and without the need of any labeling probe, the intricate sequence of protein structural changes associated with a relevant biological event. The results are further validated by characterizing the interaction between Hb and IsdB through time-resolved optical absorption (TR-OA) and fluorescence (TR-F) spectroscopy in separate stopped-flow experiments. This combined approach clarifies the structural organization of the IsdB:Hb complex upon the first encounter, to identify the principal kinetic steps leading to the formation of the final complex, and to estimate the corresponding kinetic rate constants. The resulting kinetic model brings into agreement the structural and functional insights separately collected so far[6–8,37,38]. Besides its relevance in biology and human health, this system is a challenging example of a PPI. In spite of the complexity of the IsdB:Hb interaction, we succeed in obtaining a detailed description including kinetic features, stoichiometry and cofactor transfer. Our combined approach, including static and time-resolved X-ray scattering and spectroscopy, is applicable to a broad range of biological systems and can be used to clarify the interplay between the different processes typically occurring when biomacromolecules interact.

Results

Static X-ray solution scattering

We investigated the IsdB:Hb interaction both in the SAXS and WAXS regions to better characterize the sequence of events occurring when IsdB approaches Hb, and define the structure and stoichiometry of the forming complexes. SAXS allows the characterization of the particle dimensions in solution, while WAXS is sensitive to finer structural details, thus laying the basis for the interpretation of the TR-XSS data reported below. We used two different forms of Hb to isolate key intermediates along the PPI pathway, starting with formation of an IsdB:Hb complex and leading to heme extraction to the hemophore: methemoglobin (metHb, coordinating oxidized heme) and oxyhemoglobin (oxyHb, coordinating reduced heme). While metHb, which likely represents the in vivo physiological target of *S. aureus*, allows heme extraction and transfer to IsdB[6,8,39], oxyHb does not[6], and thus offers a snapshot of the first step of the IsdB:Hb interaction.

Small angle X-ray scattering

SAXS data were collected both on IsdB:metHb and IsdB:oxyHb complexes at different concentrations (5-200 μM range). The resulting data (Fig. 2 and Supplementary Table 1) show relatively small differences in the shape of SAXS patterns as a function of the protein concentration. While the intensity at small angles slightly increases with concentration, the measured patterns are stable in time with no

https://doi.org/10.1038/s41467-024-54949-w

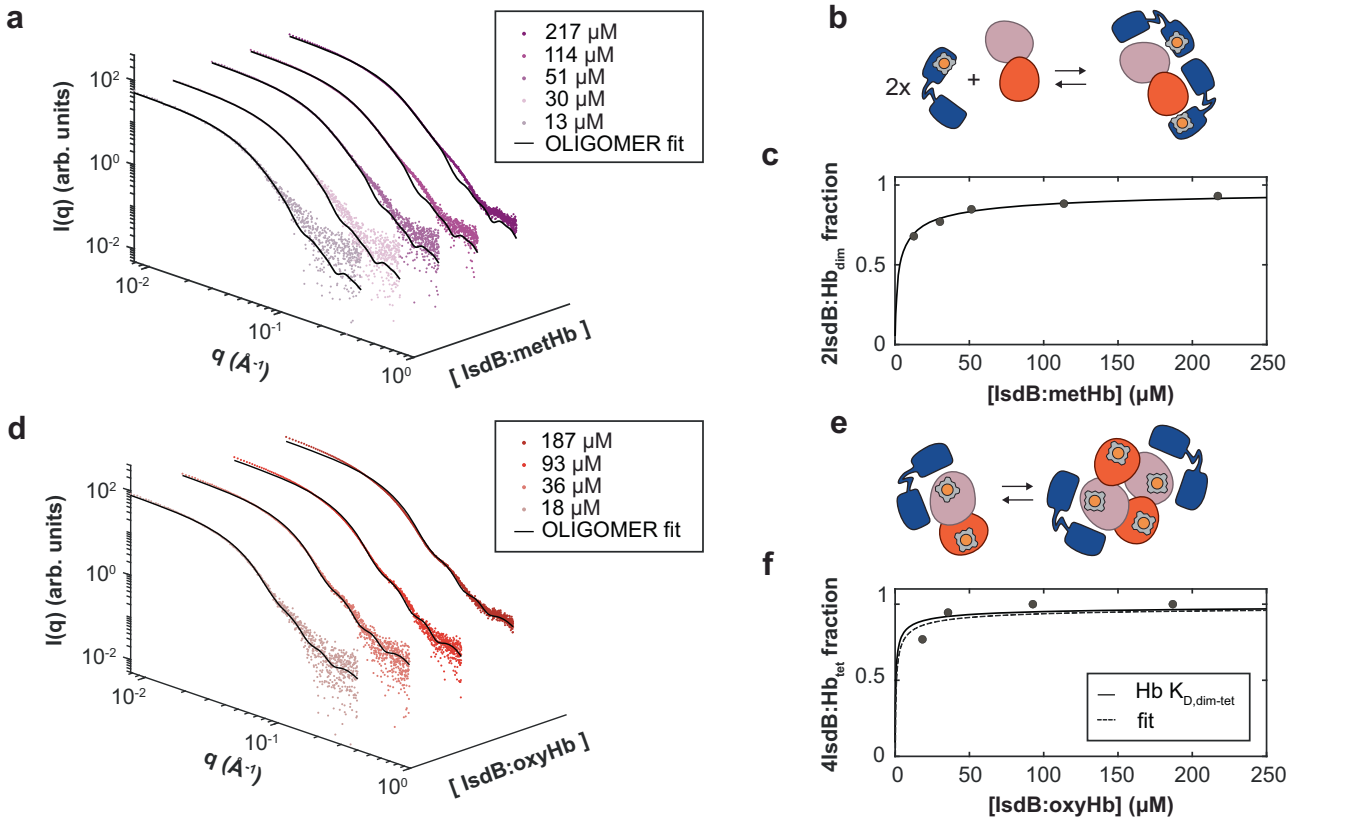

Fig. 2 | SAXS patterns of IsdB:metHb and IsdB:oxyHb complexes measured at different protein concentrations. a IsdB:metHb data (colored dots) together with fitted patterns (black solid lines) obtained with OLIGOMER. Legend reports concentrations in terms of monomeric complex (i.e. one IsdB molecule bound to a single Hb chain). **b** Schematic representation of the IsdB:metHb complex oligomeric equilibrium between IsdB molecules and metHb dimers (reagents) and two IsdB molecules bound to a metHb dimers (products, 2IsdB:metHb$_{dim}$). **c** Volume fraction of the 2IsdB:metHb$_{dim}$ extracted from the SAXS data (closed symbols, error bars defined as s.e.m. ($n = 10$) are smaller than the symbol size) plotted as a function of total IsdB:metHb concentration (monomeric complex). The fit (continuous line) yields a dissociation constant $K_D = 1.68 \pm 0.62$ μM (see "Methods" and Supplementary Text). **d** IsdB:oxyHb data (colored dots) together with fitted patterns (black solid lines) obtained with OLIGOMER. Legend reports concentrations in terms of monomeric complex (i.e. one IsdB molecule bound to an Hb dimer). **e** Schematic representation of the IsdB:oxyHb complex oligomeric equilibrium in which oxyHb dimers with a single IsdB molecule bound to their β-chain (reagent, 1IsdB:βoxyHb$_{dim}$) associate into a single particle (product, 2IsdB:βoxyHb$_{tet}$). **f** Volume fraction of the 2IsdB:βoxyHb$_{tet}$ extracted from the SAXS data (closed symbols, error bars defined as s.e.m. ($n = 10$) are smaller than the symbol size) plotted as a function of total IsdB:oxyHb concentration (monomeric complex) together with the predicted dependence in the case of simple Hb dimer-to-tetramer association using the reported dissociation constant $K_D = 0.25$ μM for oxyHb[7] (continuous line) and the fit of the data (dashed line), which yields a dissociation constant of $K_D = 0.38 \pm 1.30$ μM.

indication of large aggregates in solution. Indeed, a Guinier analysis of the data shows only a relatively small increase of the radius of gyration with sample concentration (Supplementary Fig. 1), compatible with the presence in solution of an equilibrium between species having slightly different sizes, with larger particles more abundant at higher concentrations.

Comparison of the experimental SAXS patterns (and WAXS patterns, see below) with those calculated from Protein Data Bank (PDB) structural models (Supplementary Fig. 2) of possible candidate species in IsdB:metHb mixtures, allows to unambiguously conclude that, upon interaction between IsdB and metHb, a complex made of two IsdB molecules and one metHb dimer (2IsdB:metHb$_{dim}$) is formed in solution (Supplementary Fig. 3). At the highest concentration investigated, the 2IsdB:metHb$_{dim}$ complex fully accounts for the observed X-ray pattern, while at lower concentrations an apparent lower radius of gyration is obtained, indicating the presence in solution of smaller particles. We analyzed SAXS data in terms of a linear combination of species possibly originating from 2IsdB:metHb$_{dim}$ dissociation (carried out with OLIGOMER, see "Methods"). Assuming a simple equilibrium between 2IsdB:metHb$_{dim}$, IsdB and Hb dimers, it is possible to reproduce the experimental patterns at all tested protein concentrations (Fig. 2a, b). The resulting 2IsdB:metHb$_{dim}$ volume fraction dependence on the total complex concentration yields a dissociation constant (K_D) of 1.68 ± 0.62 μM (Fig. 2c). Although the resolution of SAXS data does not allow to tell whether the heme is bound to Hb or to IsdB, the time requested for sample preparation is much higher than that needed to IsdB for extracting heme from Hb, hence we concluded that dissociation mainly occurs from a complex made of holo-IsdB (IsdB containing heme) and apo-Hb (Hb without a heme bound). Indeed, dissociation from apo-IsdB and holo-Hb is known to be in the nanomolar range[7]. Such an affinity decrease induced by heme transfer might have a physiological relevance as disengaging IsdB from Hb in vivo is a necessary step to allow the interaction of holo-IsdB with the following hemophore in the Isd iron acquisition pathway.

SAXS patterns have also been collected for IsdB:oxyHb samples, where heme extraction does not occur, in the same range of protein concentrations used for IsdB:metHb (Fig. 2d–f). The apparent radius of gyration of the complex in solution at all tested concentrations is higher than the IsdB:metHb one (Supplementary Fig. 1d). Also in this case, comparison with X-ray patterns calculated using PDB models allowed us to conclude that the majority of IsdB:oxyHb complexes in solution are composed by two IsdB molecules bound to an oxyHb tetramer (2IsdB:oxyHb$_{tet}$) (Supplementary Fig. 4f). This is in agreement with recent cryo-EM experiments indicating that two IsdB molecules

bind to the β-chains of a carbonmonoxy hemoglobin (HbCO) tetramer, when the protein concentration is relatively high (8 g/L, corresponding to 53 μM on tetramer basis)[8]. We have excluded the 2IsdB:Hb_{dim} model (Supplementary Fig. 4b) as it yields a better agreement than the 2IsdB:Hb_{tet} model mainly in the lowest q-values region, which we believe is affected by the presence of a small contamination of oligomeric species larger than any of the IsdB:Hb models (Supplementary Figs. 2 and 5, see discussion below). The 2IsdB:Hb_{tet} model has an overall better agreement through the whole region of $q > 0.05$ Å^{-1}. We have fitted the SAXS pattern at the highest protein concentration as a linear combination of the scattering patterns of the 2IsdB:oxyHb_{tet} complex, and two exceeding isolated IsdB molecules to take into account the stoichiometric ratio used to prepare the sample (see "Methods"). In view of the cryo-EM results, the 2IsdB:oxyHb_{tet} model was built so that IsdB molecules are bound to oxyHb β-chains (2IsdB:βoxyHb_{tet}). The good superposition between experimental and calculated X-ray scattering patterns (Fig. 2d) at intermediate and wide-angles (see below) supports the hypothesis that IsdB interacts with oxyHb selectively on β-subunits, as it does in the case of HbCO. Moreover, the fitting of the scattering pattern worsens when using IsdB bound to the α- rather than to the β-Hb subunits (Supplementary Fig. 5d). Although the calculated X-ray patterns are able to reproduce the data satisfactorily at q > 0.05 Å^{-1}, a worse agreement is observed at the lowest q-values. We attribute this misfit to the presence of a small fraction of oligomeric species in solution that are larger even than the fully saturated 4IsdB:Hb_{tet} model (Supplementary Fig. 2), but relatively small if compared with an extended aggregate (see "Methods" and Supplementary Fig. 5). Since heme extraction does not take place in IsdB:oxyHb complexes, we do not expect a dissociation constant of IsdB from oxyHb as high as the one that we report here for IsdB:metHb after heme extraction (1.68 μM). Moreover, oxyHb is known to undergo a tetramer-to-dimer dissociation in conditions similar to our SAXS measurements[7]. We have thus assumed that the observed concentration dependence of the IsdB:oxyHb SAXS patterns is due to the Hb dimer-to-tetramer equilibrium and analyzed the data as a linear combination of the three following species: 2IsdB:βoxyHb_{tet}, a Hb dimer with one IsdB bound to β-chains (1IsdB:βoxyHb_{dim}) and isolated IsdB molecules (Fig. 2d). The relatively good resulting fits of Fig. 2d support the hypothesis that complexes composed of oxyHb dimers with two bound IsdB molecules do not form, thus implying that dimerization is a necessary although not a sufficient condition for the binding of a second IsdB molecule (to the α-subunit), as observed in metHb.

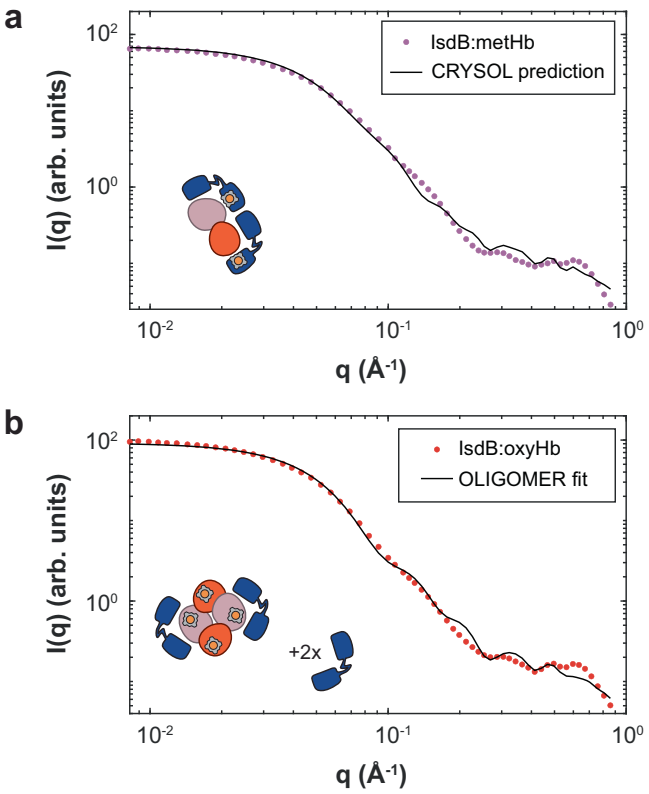

Fig. 3 | Comparison between SAXS/WAXS merged data and calculated patterns based on molecular models. a Data relative to the equilibrium complex formed by IsdB and metHb (closed symbols) vs. the 2IsdB:metHbdim calculated pattern obtained with CRYSOL (solid line). **b** Data relative to the equilibrium complex formed by IsdB and oxyHb (closed symbols) vs. the linear combination of the 2IsdB:βoxyHbtet pattern and two isolated IsdB molecules obtained with OLIGOMER (solid line, see "Methods"). Schematic representations of the molecular models used are shown in each panel. Error bars (s.e.m., $n = 10$) on experimental points are smaller than the symbol size.

Wide angle X-ray scattering

WAXS measurements have been performed on samples since they are useful for the interpretation of the time-resolved dataset presented below (collected over a comparable range of scattering angles), and are also functional to further validate the conclusions from the SAXS analysis. Indeed, a comparison between patterns calculated from structural models and experimental data extending up to the WAXS region is a much more stringent test than a comparison in the SAXS region only. In order to verify that PDB atomic models of IsdB:metHb and IsdB:oxyHb complexes accurately represent the structure of the complexes in solution, we have merged the SAXS and the WAXS static data and compared them with the solution scattering patterns calculated from PDB models. Since no significant aggregation was observed in the SAXS data over the entire range of tested concentration and in order to maximize the signal-to-noise ratio (S/N) of our data, WAXS patterns have been collected at the highest protein concentration (≈200 μM). The excellent correspondence between scattering intensities measured in the overlapping region between SAXS and WAXS, allowed us to obtain merged SAXS/WAXS patterns with remarkably good S/N in a q-range extending from 0.006 Å^{-1} to 1 Å^{-1} (Fig. 3). The calculated patterns of 2IsdB:metHb_{dim} and 2IsdB:βoxyHb_{tet} are in excellent agreement with the IsdB:metHb and IsdB:oxyHb SAXS/WAXS data, thus unambiguously confirming that these species represent the only form of the complexes present in solution (Fig. 3).

Time-resolved WAXS

The kinetics of PPI between IsdB and metHb was investigated with stopped-flow set-up for TR-XSS developed at the ID09 beamline of the ESRF (Grenoble, France) (Fig. 4). TR-XSS data have been collected in the WAXS region (TR-WAXS) after rapid mixing of IsdB and metHb solutions in equimolar concentrations (on chain basis). The total final concentration of protein was analogous to that used for static WAXS experiments (i.e., IsdB and metHb were mixed in an equimolar proportion; the final metHb concentration after mixing was 270 μM on heme basis). The stopped-flow apparatus was set so that the two solutions were fully mixed and transferred to the observation capillary within 10 ms (dead time), and at each mixing event several X-ray patterns were collected at different time-delays from mixing between 10 ms and 1 min. While the observed time window does not allow to track the earlier events of IsdB:Hb interaction, it is wide enough to monitor all the structural changes triggered by the formation of the IsdB:metHb complex.

As expected, the scattering patterns change within the observation time window, as shown in Fig. 4b, where first and last delays are depicted. Figure 4c reports the time-evolution of TR-WAXS difference patterns, i.e. the difference between the WAXS pattern measured at

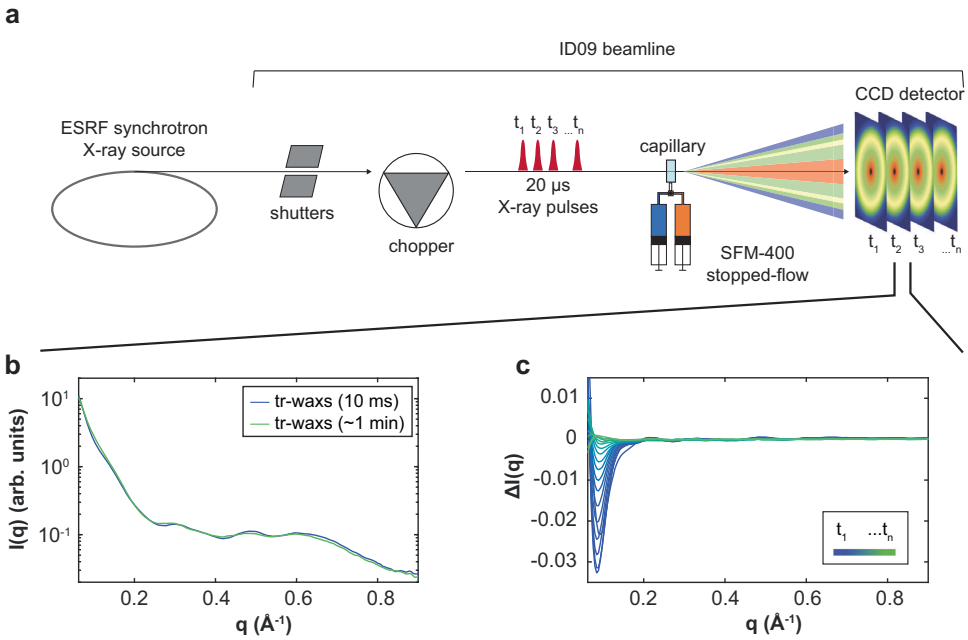

Fig. 4 | TR-XSS analysis of IsdB:metHb interaction. a Schematics of the TR-XSS setup at the ESRF ID09 beamline. X-ray solution scattering patterns are collected as a function of time after rapid mixing of an IsdB solution at a concentration of 270 μM and a Hb solution at equimolar heme concentration by means of a stopped-flow apparatus (BioLogic, SFM-4000). After the two solutions were mixed and transferred to the observation capillary, induced structural changes were probed in the sample using short X-ray pulses (pulse duration = 20 μs) isolated from the X-ray source by means of shutters and choppers. The X-ray scattering pattern generated by each pulse was recorded separately through a fast CCD detector (Rayonix MX170-HS) operated in 8×8 binning in order to achieve readout times as low as 10 ms. **b** Comparison between the WAXS pattern measured at the earliest available time point (10 ms) and at the latest one (~1 min). **c** TR-WAXS difference patterns measured at several time-delays from mixing (colormap is used to represent the time course of the reaction, where shorter delays are blue and longer ones are green).

time t from mixing and the WAXS pattern measured at the longest available time-delay from mixing (~1 min). The shape of WAXS patterns changes significantly in the investigated time frame (10 ms - 1 min), with the strongest variations being around 0.08, 0.5 and 0.65 Å^{-1}. While it is not possible to pinpoint signal changes at a given q-value to a specific structural change without further analysis, changes at 0.08 Å^{-1} are typically due to changes in the overall shape of a protein or to interactions between proteins, and changes at 0.5 and 0.65 Å^{-1} are typically arising from changes in the relative position of secondary structural elements (e.g. helices)[40]. In order to get more in-depth structural insight, we have analyzed the TR-WAXS absolute patterns (Fig. 5) in terms of an empirical kinetic model (Fig. 5c) where the only considered processes are: (1) the sequential or concurrent binding of two IsdB molecules to a metHb tetramer (2IsdB:βmetHb$_{tet}$), (2) the subsequent dimerization of the resulting complex in two metHb dimers each with a single bound IsdB molecule (1IsdB:βmetHb$_{dim}$) and (3) the binding of a second IsdB molecule to IsdB:βmetHb$_{dim}$ leading to a metHb dimer with 2 bound IsdB molecules (2IsdB:metHb$_{dim}$). We did not consider the possibility that a complex made of a Hb tetramer with 4 bound IsdB molecules is formed as such a complex would be highly unfavorable due to steric hindrance[6]. The symmetric binary model is based on complex stoichiometry observed in static SAXS/WAXS experiments on IsdB:metHb and IsdB:oxyHb. Indeed, according to the model, the interaction between IsdB and Hb initially leads to the formation of a Hb tetramer with 2 bound IsdB molecules, as in the equilibrium complex formed by IsdB and oxyHb (Fig. 3b), while a Hb dimer with 2 bound IsdB molecules is the final state when IsdB interacts with metHb (Fig. 3a). TR-WAXS data at each time delay have been fitted as a linear combination of the static pattern corresponding to the following 4 species: IsdB, Hb$_{tet}$, 2IsdB:Hb$_{tet}$, and 2IsdB:Hb$_{dim}$ (continuous lines in Fig. 5a) in order to extract the time evolution of the corresponding concentrations (closed symbols in Fig. 5b). The accumulation of intermediates whose structures are different from those collected in SAXS/WAXS static experiments is expected to result in poor data fitting. Indeed, the Hb tetramer with only one IsdB bound, transiently accumulates in the early phase of the process, but cannot be isolated in solution and the corresponding static SAXS/WAXS pattern cannot be collected. For this reason, the reported fittings in Fig. 5a started from 50 ms, since after this delay this intermediate is negligibly populated (Supplementary Fig. 6). Accordingly, for time delays longer than 50 ms the agreement between TR-WAXS experimental patterns and the corresponding fittings is satisfactory in the entire investigated scattering range (Fig. 5a).

The analysis results were globally fitted to the kinetic model reported in Fig. 5c, allowing the determination of the microscopic constants for the described molecular processes (Fig. 5b, continuous lines and Table 1). The calculated kinetic constants for the first IsdB binding to Hb (step 1), which well agree with published data[7], are also comparable to the constants for the second IsdB binding to form the final 2IsdB:metHb$_{dim}$ complex (Fig. 5c, step 3). This evidence indicates that either Hb dimerization or activation (Fig. 5c, step 2) is the rate-limiting step in the formation of the final complex. The activation process might involve a long-distance allosteric signaling that makes α-chains competent for IsdB binding with k_{on} and k_{off} values similar to those for β-chains. It should be noted that the $k_{off,1}$ and $k_{off,3}$ values are not well determined in a free fit of our data (see "Methods"). On the contrary, the k_{on} values determined from the fit are largely unaffected by the choice of k_{off} values (Supplementary Table 2).

Time-Resolved Spectroscopy

Along with TR-WAXS measurements, we performed rapid mixing stopped-flow experiments collecting time-resolved optical absorption (TR-OA) and time-resolved fluorescence (TR-F) data upon mixing IsdB and metHb solutions on a benchtop instrumentation, under the same experimental conditions used to collect the TR-WAXS dataset. Visible absorbance spectra and the single-wavelength difference signal at

https://doi.org/10.1038/s41467-024-54949-w

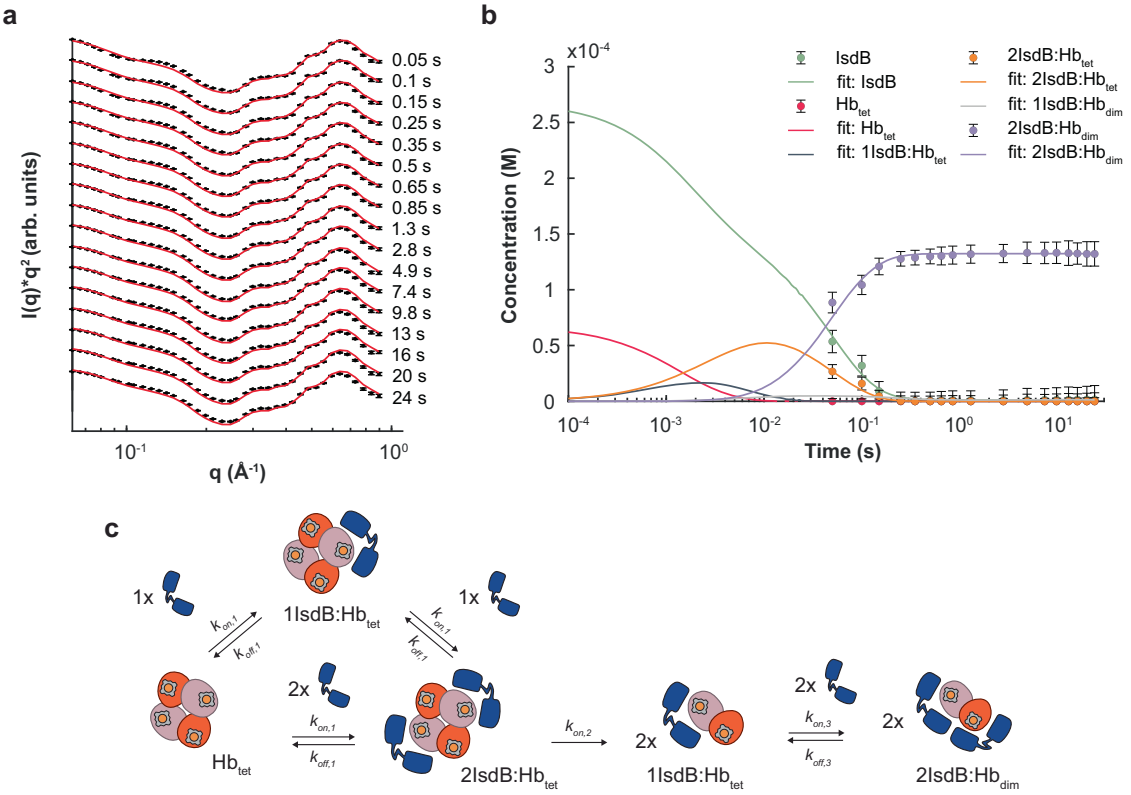

Fig. 5 | Analysis of time-resolved WAXS data in terms of a simplified kinetic model. a TR-WAXS absolute patterns (black symbols, error bars are defined as s.e.m., $n = 50$) and fittings (red lines) are plotted as $I(q)*q^2$ vs. q in order to amplify the differences between data and fittings at high q values. Fittings have been obtained in terms of the kinetic model described in the text and depicted in panel c. **b** Representation of species in IsdB:Hb complex formation estimated from the linear combination of TR-WAXS data (closed circles) in comparison with their global fitting (continuous lines). Error bars were estimated from parameter changes leading to a 2-fold increase of the reduced chi-square. **c** Kinetic model used for fitting the kinetics of species formation obtained from linear combination of TR-WAXS absolute patterns.

around 400 nm (Soret peak) probe the heme cofactor and have been used to study the heme extraction process by IsdB[5,6]. Here, we exploited a photodiode array (PDA) detector to collect spectral evolution from 1.5 ms to the end of the heme extraction process (Supplementary Fig. 7a). Singular value decomposition (SVD) was then applied to spot the two major components (Supplementary Fig. 7b), which account for 80% and 11% of the signal change, and their corresponding time courses (Fig. 6a). We also followed fluorescence emission changes of tryptophans reporting variation in their microenvironment during complex formation (Fig. 6b). We preliminarily carried out static experiments on IsdB, metHb and IsdB:metHb, finding that the fluorescence signal mainly arises from IsdB tryptophans, and shows a decrease after the interaction with Hb (Supplementary Fig. 7c).

Table 1 | Kinetic constants calculated by global data fitting to the kinetic model

STEP 1 (IsdB binding to Hb_{tet})	
$k_{on,1}$ (M^{-1} s^{-1})	$(1.4 \pm 0.8) \cdot 10^6$
$k_{off,1}$ (s^{-1})	$1 \cdot 10^{-2}$ (*)
STEP 2 (Hb dimerization / activation)	
$k_{on,2}$ (s^{-1})	20 ± 2
STEP 3 (IsdB binding to Hb_{dim})	
$k_{on,3}$ (M^{-1} s^{-1})	$(1.9 \pm 0.8) \cdot 10^6$
$k_{off,3}$ (s^{-1})	$0.5 \cdot 10^{-2}$ (*)

(*) parameters kept constant in the fitting.

In order to extract a reliable estimation of kinetic rate constants accounting for the various processes occurring after formation of a IsdB:Hb complex (including heme extraction), we have globally fitted the TR-OA and TR-F kinetics together with those obtained with TR-WAXS as a sum of exponential functions sharing the same rates (Figs. 6, Supplementary Table 3). Seven exponential functions were needed in order to obtain a good fit of the three datasets. The two slowest processes (r_6 and r_7) account for around 80% of the first SVD component of the TR-OA data (Supplementary Table 3). Since the heme chromophore is the unique contributor to absorption in the analyzed spectral range, we interpret rates 6 and 7 as mainly describing heme transfer from Hb to IsdB. The fastest of the two processes ($r_6 = 0.84\ s^{-1}$) likely represents conformational changes in the heme environment when the final complex stoichiometry has already been reached, but heme is still bound to Hb. The slowest one ($r_7 = 0.113\ s^{-1}$) is in good agreement with apparent rates already attributed to the completion of the heme transfer process[5,7]. The faster rates (r_1, r_2, r_3), are mainly associated with changes at the earliest time points of TR-OA data (second SVD component) and TR-F data. The signal changes in Trp emission (TR-F data) are mainly due to IsdB interaction with Hb (see also Supplementary Fig. 7c). On the other hand, absorbance signal (TR-OA data) is sensitive to the heme environment, thus the second SVD component likely reflects dynamics at the Hb/NEAT2 interface as sensed by the heme. The remaining r_4 and r_5 rates largely overlap in the region corresponding to Hb dimerization/activation (step 2) and subsequent IsdB binding to α-subunits. Indeed, the fourth phase (r_4) has a rate of $15.0\ s^{-1}$ while the rate obtained from the TR-WAXS data analysis is $k_{on,2} = 20\ s^{-1}$ (Table 1). Besides the values of estimated rates, we also considered their direction, and it is interesting to notice that the last

https://doi.org/10.1038/s41467-024-54949-w

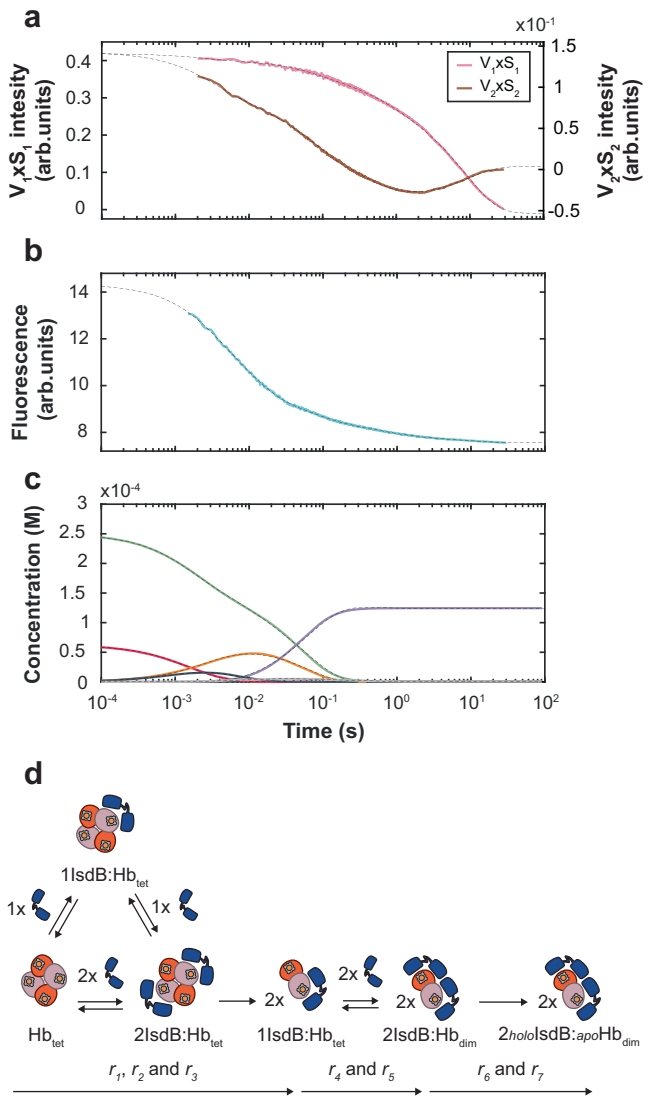

Fig. 6 | IsdB:Hb interaction followed by TR-XSS and spectroscopic techniques. Global fitting (black dashed lines) as a multiexponential function of experimental (panel **a** and **b**) and Simbiology-generated (panel **c**) data. **a** first (pink) and second (brown) SVD components from absorption spectroscopy. **b** Fluorescence (light blue) signal. **c** Simbiology-generated species concentrations: IsdB (green), Hb (red), 1IsdB:βHb$_{tet}$ complex (blue), 2IsdB:βHb$_{tet}$ complex (orange), 1IsdB:Hb$_{dim}$ complex (gray), and 2IsdB:Hb$_{dim}$ complex (purple). **d** Kinetic model used for the global fitting analysis.

kinetic phase in the second SVD component (r_7), already attributed to heme transfer to IsdB (and kinetically-associated conformational events), shows a partial reversion, suggesting that, upon heme transfer, some conformational transitions (i.e. NEAT2 domain approaching and moving away from the heme pocket) partially reverse on the same conformational path. In order to test the interpretation of the kinetic processes described above, we have performed an analogous TR-OA/TR-F stopped-flow experiment on semi-hemoglobins (semiHbs, see Supplementary Fig. 8 and Supplementary Table 4). SemiHbs are dimeric Hbs where heme is selectively bound only to α- (α-semiHb) or β-subunits (β-semiHb). Since semiHb molecules are more prone to aggregation than Hb one, experiments were carried out at a lower concentration (40 μM vs. 270 μM on globin basis). The time course of the first SVD component from TR-OA from both semiHb variants is similar to that observed for metHb (Supplementary Fig. 8 and Supplementary Table 4). A large amplitude variation, attributed to heme transfer, only occurs upon IsdB binding to both β- and α-subunits, in semiHbs as well as in metHb. This evidence supports the hypothesis that IsdB likely interacts with β-subunits in all Hb variants, regardless of their holo- or apo-forms, with comparable rates, and heme extraction occurs only when both subunits in a Hb dimer are bound to IsdB. Moreover, since semiHbs are dimeric, we demonstrated that Hb dimerization, while a necessary step for making α-subunit competent towards IsdB binding, is not the rate limiting event, but a process faster than, or rate-limited by, β-α intersubunit communication. Considering that a rate in the order of 10^{-3} s^{-1} has been reported for the Hb tetramer dissociation into dimers[41,42], we can conclude that IsdB binding to β-subunits promotes faster metHb dimerization by several orders of magnitude, while this effect was not observed in oxyHb. These data confirmed that heme oxidation increases protein dynamics, causing a faster dimerization, and eventually activating α subunits competence for IsdB binding. Also fluorescence time-courses are comparable for metHb and semiHbs, again supporting that IsdB first binds β- and then α-subunits regardless of the presence or absence of the heme cofactor (Supplementary Fig. 8). SemiHbs do not significantly differ from metHb in terms of rates also in the second SVD component from TR-OA, but they have a much smaller amplitude in the faster rates preceding heme transfer (Supplementary Table 4). We attributed this component to dimerization or conformational changes such as inter-dimer activation directly sensed by the heme. In semiHbs this process is not occurring and this could explain the reduced amplitude.

Discussion

By integrating static and TR-XSS, with TR-OA and TR-F spectroscopy, we were able to dissect the complex stoichiometry, the Hb oligomerization state, and the kinetics along the reaction pathway following the interaction between IsdB and Hb and leading to heme extraction: IsdB binding to oxyHb β-subunits does not significantly destabilize Hb tetramers, and dimerization is a necessary but not sufficient condition for a second IsdB binding. This latter event only occurs on metHb, where intersubunit communications triggered by IsdB binding to β-chains make α-subunits competent for IsdB binding. Only when both globin chains on a Hb dimer are bound to IsdB, heme extraction proceeds. We challenged our kinetic model and microscopic constants for their ability to predict how IsdB and Hb interact in different experimental conditions. The good agreement between the rate constants from our simulation and published ones[6] (Supplementary Figs. 9 and Supplementary Table 5) proves that the approach we developed can be confidently used to describe the in vitro behavior of IsdB:metHb PPI. These findings can be evaluated in view of their physiological meaning and implications. Hb free in the plasma from hemolyzed red blood cells circulates mainly as dimers, and IsdB can bind dimers or tetramers on β-subunits with the same efficiency. Binding of a second IsdB molecule present in a spatial proximity is then required to trigger concomitant heme extraction. This would guarantee a fully productive interaction of the bacterium with the iron-containing protein. This mechanism implies that IsdB molecules are anchored to the cell wall at a distance suitable for forming a ternary complex. This could be expected considering the necessary colocalization of other proteins of the Isd system, such as IsdA, to allow heme transfer and internalization, and the observed surface distribution of IsdB (and IsdA) under iron starvation conditions that localize to discrete puncta throughout the cell surface[43]. Besides biological implications of this mechanism, these findings possibly contribute to the design of inhibitors of the interaction between IsdB and Hb as a way to bacterial iron starving. In particular, our results suggest that inhibition strategies do not necessarily need to aim at blocking the initial binding event of IsdB to Hb β-chains, but can also target the subsequent binding of IsdB to Hb α-chains, which anyway precedes heme extraction. In this study, we coupled rapid mixing TR-WAXS with structural and spectroscopic analyses, which can attribute structural determinants to microscopic

kinetic constants, with the aim of studying not a single molecular entity but a higher complexity system, i.e. the characterization of structural dynamics following protein-protein interactions.

Methods

Proteins expression and purification

Expression and purification of StrepTag®II-IsdB and purification of human Hb were carried out as described in Supplementary Methods[7,8,44]. Human Hb was purified from outdated blood donated to a transfusion center by volunteers, from whom written informed consent was obtained. Both the blood donation and use of outdated samples were performed in accordance with Italian law on blood donation and usage (Italian law 219/2005). All protein samples used for the analysis were dialyzed against the experimental buffer containing 100 mM Tris/HCl, 150 mM NaCl, and 1 mM EDTA, pH 8.0, flash-frozen in liquid nitrogen, and stored at −80 °C.

Static X-ray solution scattering data collection

Static SAXS and WAXS data were collected at the BM29 beamline and at the ID09 beamline of the ESRF, respectively. Several preliminary measurements were carried out to find optimal working conditions in terms of solvent composition and pH. The exposure time has been adjusted to make sure that X-ray-induced radiation damage was negligible. For SAXS data collection an X-ray energy of 12.5 keV and a sample-to-detector distance of 2.849 m were used, while WAXS data were collected at 17.45 keV and 0.39 m. In both cases, approximately 50 µL of each sample was loaded into a 1.7 mm quartz glass capillary. Immediately before the data collection, samples were centrifuged at 17,200 g for 30 min at 4 °C and the supernatant was collected and loaded into the sample exchanger after checking its optical absorption spectrum with a Nanodrop spectrometer (Thermo Scientific). The protein concentration ranged from 12 to 220 µM for SAXS and from 90 to 270 µM for WAXS measurements. SAXS data were collected using a Pilatus 1 M detector at an exposure of 0.5 s per image while the sample was flowing through the capillary at a flow speed of 5 µL/s. WAXS data were collected using a Rayonix MX170-HS detector exposing the sample to short (~3 µs) X-ray pulses at a repetition rate of 10 Hz while the sample was translated in steps of 60 µm in between two consecutive X-ray pulses. Microsecond X-ray pulses were selected using a high-speed chopper operated in the so-called tunnel-less mode[45]. Typically, 10 images per sample were azimuthally integrated using pyFAI in order to obtain the scattering intensity as a function of the scattering vector magnitude $q = 4\pi\sin(\theta)/\lambda$, where 2θ is the scattering angle and λ is the X-ray scattering wavelength. Scattering patterns from the same sample were averaged together after verifying that they were perfectly superimposable. Buffer data were collected before and after each protein sample and used as a reference to calculate the protein excess scattering signal. All data were collected using standard software available at the ESRF (CSS SPEC ver. 6.0). The protein radius of gyration (R_g) was estimated from the SAXS data either by the automatic software available at the BM29 beamline or by custom Python scripts. WAXS data were collected at the highest protein concentration at which SAXS data show minimal sign of protein aggregation or interparticle interference effect. SAXS and WAXS data were then merged and rebinned so that experimental points were homogeneously spaced on a logarithmic q-scale. Error bars on reduced data were calculated as standard error of the mean (s.e.m.).

Modeling of X-ray solution scattering data

In order to extract structural information from the SAXS/WAXS data we compared experimental patterns with curves calculated from structural models using CRYSOL[46]. Analogous results were obtained using a software that takes the hydration shell explicitly into account like WAXSiS[47] (Supplementary Fig. 10). We have used CRYSOL for further analysis in order to have a more direct comparison with the results obtained with OLIGOMER (see below). We considered all possible a priori candidate models (Supplementary Fig. 2) of the IsdB:Hb complex starting from a metHb monomer bound to a single IsdB molecule up to a Hb tetramer bound to four IsdB molecules. All models have been generated starting from the available crystallographic structure of *S. aureus* IsdB bound to human Hb (PDB ID 5VMM) where the Hb component was replaced by a high resolution metHb crystallographic structure (PDB ID 3P5Q). The I-TASSER web server[48] was used to model the missing StrepTag®II in the 5VMM PDB model. A full metHb tetramer with 4 bound IsdB molecules (4IsdB:Hb_{tet}) was thus generated and all subsequent models were obtained by removing elements. Thus, the 2IsdB:Hb_{dim} was generated by removing one Hb dimer with the two bound IsdBs, the 1IsdB:Hb_{dim} was generated by removing an additional IsdB and so on. By directly comparing the experimental SAXS/WAXS patterns with each of the above models (Supplementary Figs. 3 and 4), it was possible to exclude several possible candidate structures.

Fitting of SAXS dilution series

An overall good agreement with the IsdB:metHb SAXS dilution series (Fig. 2a) can be obtained using a model containing a metHb dimer and 2 bound IsdB molecules (Supplementary Fig. 2). However, small deviations were observed especially when the calculated patterns were compared with the data measured at the lowest protein concentration. We have fitted the SAXS data, to consider possible dissociation equilibria, as a linear combination of IsdB, Hb_{dim}, 1IsdB:αHb_{mon}, 1IsdB:βHb_{mon}, IsdB:Hb_{dim} models (Supplementary Fig. 2) using OLIGOMER[49]. Volume fractions of models were constrained so that 2IsdB:metHb_{dim} dissociate into one Hb dimer and two IsdB molecules or IsdB bound to single Hb chains. Data corresponding to IsdB:oxyHb sample were found to best fit using models made of two IsdB molecules bound to the α- or the β-chains of an Hb tetramer (2IsdB:αHb_{tet} or 2IsdB:βHb_{tet}), with model 2IsdB:βHb_{tet} giving a best fit agreement (Supplementary Fig. 5b). Even in the SAXS series of this complex, data measured at lower protein concentration showed deviations from the theoretical curve. In this case, OLIGOMER fits of the SAXS data at different concentrations have been performed as linear combinations of the above pattern (model 2IsdB:βHb_{tet}), the pattern of one IsdB bound to the β-chains of an Hb dimer (model 1IsdB:βHb_{dim}), and the pattern of isolated IsdB. The reason why this latter structure was included is to consider the 1:1 globin chain:IsdB stoichiometric ratio of the mixture prepared for scattering experiments, and the same ratio was constrained throughout OLIGOMER analysis (namely one isolated IsdB for each 1IsdB:βHb_{dim} and two isolated IsdB for each 2IsdB:βHb_{tet}). Also in this case, adding models of the isolated proteins or the complex in a different stoichiometric ratio (namely model 2IsdB:Hb_{dim}) (Supplementary Fig. 5a) did not improve OLIGOMER fits. Finally, theoretical patterns of the above-selected models or model mixtures were compared to the merged SAXS/WAXS patterns of both IsdB:metHb and IsdB:oxyHb, which define the analyzed sample with higher resolution, to further confirm the achieved results. SAXS concentration series of both IsdB:Hb complexes were fitted using OLIGOMER to determine the change in the oligomeric state of Hb within the two complexes (IsdB:metHb and IsdB:oxyHb). The dissociation constant for the above equilibrium was calculated adapting the equation reported previously[50], see Supplementary Methods.

TR-WAXS data collection

TR-WAXS data were collected at the ID09 beamline of the ESRF. Samples were prepared similarly to those used for the static SAXS and WAXS data collections. Solutions of human metHb and *S. aureus* IsdB were loaded into two different syringes of an SFM-4000 BioLogic stopped-flow apparatus equipped with a 1.4 mm quartz glass capillary. In order to get a final equimolar concentration of 270 µM, 28 µL of the metHb solution (954 µM) was

mixed with 72 µL of the IsdB solution (371 µM). The flow rate of mixing (1.67 mL/s) was optimized in order to minimize any inhomogeneity of the sample and corresponds to a dead time of 10 ms. X-ray scattering patterns in the 0.05-2.2 $Å^{-1}$ scattering region were recorded with a Rayonix MX170-HS detector at an X-ray energy of 17.67 keV and a sample-to-detector distance of 0.4 m. Each image is the result of the interaction of the sample with a single 20 µs X-ray pulse. At each mixing event, up to 24 images were recorded at different time delays from mixing between 10 ms and 1 min. By operating the Rayonix detector in frame-transfer mode and 8 × 8 binning, it was possible to record consecutive images every 30 ms in the fast part of the kinetics. Preliminary measurements were used to optimize the exposure time per image and the total number of images per mixing event so as to minimize any heating or radiation damage effect on the sample. All data collections were performed using CSS SPEC ver. 6.0. TR-WAXS images were azimuthally averaged using pyFAI and the resulting 1D curves were normalized in the 2.1–2.2 $Å^{-1}$ water scattering region before further processing to correct for fluctuations in the intensity of the X-ray beam[13] using the Python package txs (https://gitlab.esrf.fr/levantin/txs). The data collection sequence was repeated for at least 50 times and TR-WAXS patterns at the same time-delay were averaged together to increase the signal-to-noise ratio of the dataset. The resulting S(q, t) patterns were used to calculate TR-WAXS difference patterns as ΔS(q, t) = S(q, t) - S(q, 1 min), i.e. the WAXS pattern measured at the longest available time delay (1 min) was used as a reference. TR-WAXS absolute patterns were instead obtained as S(q, t) - S_{buffer}(q), where S_{buffer}(q) is the equilibrium WAXS pattern of the buffer solution measured with the same stopped-flow apparatus used for the TR-WAXS data collection. TR-WAXS absolute patterns are thus proportional to the excess protein scattering contribution and directly comparable to the static XSS data. Error bars were calculated as s.e.m. for all patterns.

TR-WAXS data analysis

The data analysis reported in the main text is focused on the 0.05–1 $Å^{-1}$ q-range where pattern changes are expected to originate mainly from stoichiometry changes and tertiary rearrangements. Patterns changes in the 1–2.2 $Å^{-1}$ range are dominated by changes in the solvent structure around the IsdB:Hb complex induced by heat transfer between the protein complex and the solvent (Supplementary Fig. 11). The theoretical WAXS pattern for each time delays, S_{theo}, can be written as linear combination of experimental static WAXS scattering patterns, S, of isolated proteins, IsdB:oxyHb complex, and IsdB:metHb complex:

$$S_{theo} = W_{IsdB} \cdot S(IsdB) + W_{Hb_{tet}} \cdot S(Hb_{tet}) + W_{IsdB:oxyHb} \cdot S(IsdB:oxyHb) + W_{IsdB:metHb} \cdot S(IsdB:metHb) \quad (1)$$

weight vectors for each molecular species over time were obtained using a least-squares fit by comparing the experimental TR-WAXS pattern at each time delay with the theoretical pattern (S_{theo}) using the Fminuit minimization algorithm in MATLAB. The minimization was only constrained to keep weights of isolated proteins constant over time to take into account the stoichiometric ratio used to prepare the sample. During the fitting step, the IsdB weight was calculated as follows:

$$W_{IsdB(tot)} = W_{IsdB} + 2 \cdot W_{IsdB:oxyHb} \quad (2)$$

since the scattering pattern of IsdB:oxyHb complex describes a sample where a mixture of 2IsdB:Hb_{tet} complex and 2-times molar excess of IsdB are present in solution (as discussed in the Results section). Weights were normalized by dividing each value by the one of IsdB:metHb complex at the last delay (which is the only species present at the end of the reaction). Normalized weights were then multiplied by 135 µM, which is the concentration of the final complex in our experimental conditions, to obtain concentrations of different species over time. This linear combination was carried out on the complete dataset and the resulting weight vectors over time were used as input to SimBiology[51] to extrapolate microscopic constants for the molecular processes involved in IsdB:metHb protein-protein interaction and to simulate the time evolution of the concentration of molecular species. We performed the global fit of TR-WAXS datasets employing nonlinear regressions statistical model, Fmincon as local solver and scatter search as global solver, a proportional error model for each molecular species and by pooling all estimated parameters together. Since the analysis of TR-WAXS patterns has been performed at time delays longer than 50 ms, the parameters $k_{off,1}$ and $k_{off,3}$ could not be well determined by the fitting process. After performing an initial SimBiology fit data run, in which published data[6] were used as initialization value, a second fitting run was performed with $k_{off,1}$ and $k_{off,3}$ fixed at the best-fit values obtained in the first round. A different choice of $k_{off,1}$ and $k_{off,3}$ values minimally affects the best fit values obtained for the other parameters (Supplementary Table 2). Errors on the fitting parameters reported in Table 1 correspond to parameter changes resulting in an increase of the reduced chi-square by a factor 2. An SVD analysis was also performed on the data reported in Fig. 5a and shows that at least 3 exponential functions are needed to explain the time-dependence of the TR-WAXS data (Supplementary Fig. 12).

TR-OA and TR-F spectroscopy

TR-OA and TR-F experiments were carried out using an SX18 stopped-flow apparatus (Applied Photophysics) with a dead time of about 1.5 ms equipped with a 150 W xenon lamp and alternatively coupled to a photomultiplier for fluorescence spectroscopy or to an SX Direct Coupled Photodiode Array Detector for multi-wavelength absorption measurement. The stopped-flow data acquisition was performed using Applied Photophysics Pro-Data SX. The kinetics of the reaction between equimolar amounts of IsdB and metHb (globin concentration) at concentration mimicking TR-WAXS experiments (250 µM of IsdB and metHb) or at lower concentration (40 µM IsdB and Hb) were measured at 20 °C in the experimental buffer. The interaction between IsdB and semiHbs was assessed to kinetically evaluate whether the hemophore interaction with Hb is affected by the absence of heme. Since semiHbs appeared unstable under the TR-WAXS experimental conditions (namely, 270 µM globin concentration), we tested this reaction by mixing equimolar concentrations of IsdB and semi(α) or semi(β)metHb at a concentration of 40 µM. For the experiment mimicking the TR-WAXS conditions, we have collected spectroscopic data in the Q bands (525-700 nm), while for the semiHbs, we have used the Soret band (380–450 nm). The typical peak absorbances of our samples in both cases were approximately 0.8 OD. In these conditions, the instrumental error on the absorbance signal is 0.002 OD. Fluorescence emission (298 nm excitation) was recorded at 90° after passing through a 320 nm cut-off filter by acquiring 10,000 data points for up to 30 s. For rapid-scanning experiments, 1,000 logarithmically spaced spectra of the reaction mixture (in the 320–700 nm interval) were collected for up to 30 s. For the stopped-flow fluorescence experiments, we have estimated the average relative error on the measurements to be of the order of 3% by evaluating the deviation of the data with respect to smoothed data (Savitzy-Golay filter).

Global fitting of kinetic data

Global fitting was performed adapting lsqmultinonlin function[52]. Time courses of concentration for molecular species simulated by SimBiology Model Analyzer, absorbance and fluorescence spectroscopy were fitted with a sum of seven or six exponential functions. The

amplitudes of the signals were left free to change while the exponential rates (r_1–r_7) were kept constant throughout the entire dataset. All the above data analysis steps were performed with MATLAB R2021a.

Reporting summary

Further information on research design is available in the Nature Portfolio Reporting Summary linked to this article.

Data availability

The dataset generated and analyzed in this study has been deposited in the Figshare[53] database under accession code https://doi.org/10.6084/m9.figshare.25524796. Crystallographic models used in this study are available under accession code 5VMM (Staphylococcus aureus IsdB bound to human Hb) and 3P5Q (high-resolution R-state human Hb).

Code availability

Codes generated during the current study are available from the corresponding authors on request.

References

1. Lowy, F. D. How *Staphylococcus aureus* adapts to its host. *N. Engl. J. Med.* **364**, 1987–1990 (2011).
2. Mazmanian, S. K. et al. Passage of heme-iron across the envelope of *Staphylococcus aureus*. *Science* **299**, 906–909 (2003).
3. Torres, V. J. et al. *Staphylococcus aureus* IsdB is a hemoglobin receptor required for heme iron utilization. *J. Bacteriol.* **188**, 8421–8429 (2006).
4. Pishchany, G. et al. IsdB-dependent hemoglobin binding is required for acquisition of heme by *Staphylococcus aureus*. *J. Infect. Dis.* **209**, 1764–1772 (2014).
5. Zhu, H. et al. Non-heme-binding domains and segments of the *Staphylococcus aureus* IsdB protein critically contribute to the kinetics and equilibrium of heme acquisition from methemoglobin. *PLoS One* **9**, e100744 (2014).
6. Bowden, C. F. M. et al. Structure–function analyses reveal key features in *Staphylococcus aureus* IsdB-associated unfolding of the heme-binding pocket of human hemoglobin. *J. Biol. Chem.* **293**, 177–190 (2018).
7. Gianquinto, E. et al. Interaction of human hemoglobin and semihemoglobins with the *Staphylococcus aureus* hemophore IsdB: a kinetic and mechanistic insight. *Sci. Rep.* **9**, 18629 (2019).
8. De Bei, O. et al. Cryo-EM structures of staphylococcal IsdB bound to human hemoglobin reveal the process of heme extraction. *Proc. Natl Acad. Sci. USA* **119**, e2116708119 (2022).
9. Tacconelli, E. et al. Discovery, research, and development of new antibiotics: the WHO priority list of antibiotic-resistant bacteria and tuberculosis. *Lancet Infect. Dis.* **18**, 318–327 (2018).
10. Beyer, P. & Paulin, S. Priority pathogens and the antibiotic pipeline: an update. *Bull. World Health Organ.* **98**, 151 (2020).
11. Levantino, M. et al. Using synchrotrons and XFELs for time-resolved X-ray crystallography and solution scattering experiments on biomolecules. *Curr. Opin. Struct. Biol.* **35**, 41–48 (2015).
12. Cho, H. S. et al. Time-resolved X-ray scattering studies of proteins. *Curr. Opin. Struct. Biol.* **70**, 99–107 (2021).
13. Cammarata, M. et al. Tracking the structural dynamics of proteins in solution using time-resolved wide-angle X-ray scattering. *Nat. Methods* **5**, 881–886 (2008).
14. Cammarata, M. et al. Unveiling the timescale of the R–T transition in human hemoglobin. *J. Mol. Biol.* **400**, 951–962 (2010).
15. Levantino, M. et al. The Monod-Wyman-Changeux allosteric model accounts for the quaternary transition dynamics in wild type and a recombinant mutant human hemoglobin. *Proc. Natl Acad. Sci. USA* **109**, 14894–14899 (2012).
16. Andersson, M. et al. Structural dynamics of light-driven proton pumps. *Structure* **17**, 1265–1275 (2009).
17. Malmerberg, E. et al. Time-resolved WAXS reveals accelerated conformational changes in iodoretinal-substituted proteorhodopsin. *Biophys. J.* **101**, 1345–1353 (2011).
18. Cho, H. S. et al. Protein structural dynamics in solution unveiled via 100-ps time-resolved x-ray scattering. *Proc. Natl Acad. Sci. USA* **107**, 7281–7286 (2010).
19. Levantino, M. et al. Ultrafast myoglobin structural dynamics observed with an X-ray free-electron laser. *Nat. Commun.* **6**, 6772 (2015).
20. Brinkmann, L. U. L. & Hub, J. S. Ultrafast anisotropic protein quake propagation after CO photodissociation in myoglobin. *Proc. Natl Acad. Sci. USA* **113**, 10565–10570 (2016).
21. Björling, A. et al. Structural photoactivation of a full-length bacterial phytochrome. *Sci. Adv.* **2**, 1600920 (2016).
22. Heyes, D. J. et al. Light-induced structural changes in a full-length cyanobacterial phytochrome probed by time-resolved X-ray scattering. *Commun. Biol.* **2**, 1 (2019).
23. Berntsson, O. et al. Sequential conformational transitions and α-helical supercoiling regulate a sensor histidine kinase. *Nat. Commun.* **8**, 284 (2017).
24. Josts, I. et al. Photocage-initiated time-resolved solution X-ray scattering investigation of protein dimerization. *IUCrJ* **5**, 667–672 (2018).
25. Ravishankar, H. et al. Tracking Ca2+ ATPase intermediates in real time by x-ray solution scattering. *Sci. Adv.* **6**, eaaz0981 (2020).
26. Orädd, F. et al. Tracking the ATP-binding response in adenylate kinase in real time. *Sci. Adv.* **7**, eabi5514 (2021).
27. Rimmerman, D. et al. Direct observation of insulin association dynamics with time-resolved X-ray scattering. *J. Phys. Chem. Lett.* **8**, 4413–4418 (2017).
28. Rimmerman, D. et al. Insulin hexamer dissociation dynamics revealed by photoinduced T-jumps and time-resolved X-ray solution scattering. *Photochem. Photobiol. Sci.* **17**, 874–882 (2018).
29. Cho, H. S. et al. Dynamics of quaternary structure transitions in R-state carbonmonoxyhemoglobin unveiled in time-resolved X-ray scattering patterns following a temperature jump. *J. Phys. Chem. B* **122**, 11488–11496 (2018).
30. Thompson, M. C. et al. Temperature-jump solution X-ray scattering reveals distinct motions in a dynamic enzyme. *Nat. Chem.* **11**, 1058–1066 (2019).
31. Hsu, D. J. et al. Unfolding bovine α-lactalbumin with T-jump: characterizing disordered intermediates via time-resolved x-ray solution scattering and molecular dynamics simulations. *J. Chem. Phys.* **154**, 105101 (2021).
32. Akiyama, S. et al. Conformational landscape of cytochrome c folding studied by microsecond-resolved small-angle x-ray scattering. *Proc. Natl Acad. Sci. USA* **99**, 1329–1334 (2002).
33. Arai, M. et al. Microsecond hydrophobic collapse in the folding of *Escherichia coli* dihydrofolate reductase, an α/β-type protein. *J. Mol. Biol.* **368**, 219–229 (2007).
34. West, J. M. et al. Time evolution of the quaternary structure of *Escherichia coli* aspartate transcarbamoylase upon reaction with the natural substrates and a slow, tight-binding inhibitor. *J. Mol. Biol.* **384**, 206–218 (2008).
35. Konuma, T. et al. Time-resolved small-angle X-ray scattering study of the folding dynamics of barnase. *J. Mol. Biol.* **405**, 1284–1294 (2011).
36. Josts, I. et al. Structural kinetics of MsbA Investigated by stopped-flow time-resolved small-angle X-ray scattering. *Structure* **28**, 348–354.e3 (2020).
37. Gaudin, C. F. M. et al. Unique heme-iron coordination by the hemoglobin receptor IsdB of *Staphylococcus aureus*. *Biochemistry* **50**, 5443–5452 (2011).
38. Fonner, B. A. et al. Solution structure and molecular determinants of hemoglobin binding of the first NEAT domain of IsdB in *Staphylococcus aureus*. *Biochemistry* **53**, 3922–3933 (2014).

39. Bowden, C. F. M. et al. Hemoglobin binding and catalytic heme extraction by IsdB near iron transporter domains. *Biochemistry* **53**, 2286–2294 (2014).
40. Hirai, M. et al. Structural hierarchy of several proteins observed by wide-angle solution scattering. *J. Synchrotron Rad.* **9**, 202–205 (2002).
41. Romeo, P. H. et al. Kinetics of subunit dissociation of partially oxygenated hemoglobin determined by haptoglobin binding. *Biochem. Biophys. Res. Commun.* **105**, 1354–1360 (1982).
42. Ip, S. H. et al. Kinetics of deoxyhemoglobin subunit dissociation determined by haptoglobin binding: estimation of the equilibrium constant from forward and reverse rates. *Biochemistry* **15**, 654–660 (1976).
43. Pishchany, G. et al. Subcellular localization of the *Staphylococcus aureus* heme iron transport components IsdA and IsdB. *Infect. Immun.* **77**, 2624–2634 (2009).
44. Cassoly, R. & Banerjee, R. Structure and function of human semihemoglobins alpha and beta. *Eur. J. Biochem.* **19**, 514–522 (1971).
45. Cammarata, M. et al. Chopper system for time-resolved experiments with synchrotron radiation. *Rev. Sci. Instrum.* **80**, 015101 (2009).
46. Franke, D. et al. ATSAS 2.8: a comprehensive data analysis suite for small-angle scattering from macromolecular solutions. *J. Appl. Crystallogr.* **50**, 1212–1225 (2017).
47. Knight, C. J. & Hub, J. S. WAXSiS: a web server for the calculation of SAXS/WAXS curves based on explicit-solvent molecular dynamics. *Nucl. Acids Res.* **43**, W225–W230 (2015).
48. Yang, J. & Zhang, Y. I-TASSER server: new development for protein structure and function predictions. *Nucl. Acids Res.* **43**, W174–W181 (2015).
49. Konarev, P. V. et al. PRIMUS: a Windows PC-based system for small-angle scattering data analysis. *J. Appl. Crystallogr.* **36**, 1277–1282 (2003).
50. Jarmoskaite, I. et al. How to measure and evaluate binding affinities. *Elife* **9**, e57264 (2020).
51. The MathWorks Inc. SimBiology version: 6.1 (R2021a), Natick, Massachusetts: The MathWorks Inc. https://www.mathworks.com (2023).
52. Al-Jewad, B. lsqmultinonlin global parametric nonlinear regression with shared parameters, https://www.mathworks.com/matlabcentral/fileexchange/68727-lsqmultinonlin (2023).
53. De Bei, O. et al. "Time-resolved X-ray solution scattering unveils the events leading to hemoglobin heme capture by staphylococcal IsdB" [Dataset]. *Figshare* https://doi.org/10.6084/m9.figshare.25524796 (2024).

Acknowledgements

We acknowledge the European Synchrotron Radiation Facility (ESRF) for provision of beamtime (proposals IH-LS-3074 and LS-2807) at the ID09 and BM29 beamlines. For the experiments performed at the ESRF, we kindly acknowledge Petra Pernot and Gabriele Giachin for assistance in using BM29 and Pierre Lloria for assistance in using the Partnership for Soft Condensed Matter (PSCM) laboratories. This work was supported through PRIN 2020AE3LTA "DEfeat antimicrobial ResistAnce through iron starvation in *Staphylococcus aurEus* (ERASE)" Italian Ministry of University and Research (to SB), PRIN 2022RCP52Y "BIOMHEME - A biomimetic approach to remove free hemoglobin from plasma inspired by bacterial iron capturing systems" Italian Ministry of University and Research (to LR and SG), local funding from the University of Parma ("Scientific Equipment Fund", for SX-18 Applied Photophysics stopped flow upgrade (to SB, LR and BC) and ESRF inhouse research budget (to ML). ODB was supported by the fellowship "Lascito Feliciani-Ferretti anno 2022". We thank Dr. Manuele Bettelli (IMEM-CNR) and Prof. Stefania Abbruzzetti (University of Parma) for helpful discussion and technical support preparing MATLAB scripts.

Author contributions

S.B., M.L., and L.R. conceived the project. M.L. and L.R. coordinated the project. O.D., M.M., M.L., and L.R. performed the static and time-resolved X-ray solution scattering experiments. O.D. and M.M. prepared and tested basic functionalities of the proteins used in this study. O.D. and L.R. performed the time-resolved spectroscopic measurements. S.G., E.G., and F.S. prepared the PDB models used to fit the X-ray solution scattering data. O.D., M.L., and L.R. analyzed all data and wrote the manuscript, with a critical reading from B.C. and contributions from all the authors. All authors have approved the final version of the manuscript.

Competing interests

The authors declare no competing interests.

Additional information

Supplementary information The online version contains supplementary material available at https://doi.org/10.1038/s41467-024-54949-w.

Correspondence and requests for materials should be addressed to Matteo Levantino or Luca Ronda.

Peer review information *Nature Communications* thanks Hyotcherl Ihee, Irina Kosheleva and the other, anonymous, reviewer for their contribution to the peer review of this work. A peer review file is available.